NMR Solution Structure of Attractin, a Water-Borne Protein Pheromone from the Mollusk Aplysia californica †

ARTICLE *in* BIOCHEMISTRY · SEPTEMBER 2003

Impact Factor: 3.02 · DOI: 10.1021/bi0274322 · Source: PubMed

7 AUTHORS, INCLUDING:

Catherine H Schein
Foundation for Applied Molecular Evolution
117 PUBLICATIONS **2,810** CITATIONS
SEE PROFILE

Krishna Rajarathnam
University of Texas Medical Branch at Galves…
65 PUBLICATIONS **2,664** CITATIONS
SEE PROFILE

Werner Braun
University of Texas Medical Branch at Galves…
145 PUBLICATIONS **11,340** CITATIONS
SEE PROFILE

NMR Solution Structure of Attractin, a Water-Borne Protein Pheromone from the Mollusk *Aplysia californica*†

Ravindranath Garimella,‡ Yuan Xu,‡ Catherine H. Schein,‡ Krishna Rajarathnam,‡ Gregg T. Nagle,§ Sherry D. Painter,§ and Werner Braun*,‡

Sealy Center for Structural Biology, Department of Human Biological Chemistry and Genetics, and The Marine Biomedical Institute and Department of Anatomy and Neurosciences, University of Texas Medical Branch, Galveston, Texas 77555

Received December 31, 2002; Revised Manuscript Received June 16, 2003

ABSTRACT: Water-borne protein pheromones are essential for coordination of reproductive activities in many marine organisms. In this paper, we describe the first structure of a pheromone protein from a marine organism, that of attractin (58 residues) from *Aplysia californica*. The NMR solution structure was determined from TOCSY, NOESY, and DQF-COSY measurements of recombinant attractin expressed in insect cells. The sequential resonance assignments were done with standard manual procedures. Approximately 90% of the 949 unambiguous NOESY cross-peaks were assigned automatically with simultaneous three-dimensional structure calculation using our NOAH/DIAMOD/FANTOM program suite. The final bundle of energy-refined structures is well-defined, with an average rmsd value to the mean structure of 0.72 ± 0.12 Å for backbone and 1.32 ± 0.11 Å for heavy atoms for amino acids 3−47. Attractin contains two antiparallel helices, made up of residues Ile9−Gln16 and I30−S36. The NMR distance constraints are consistent with the three disulfide bonds determined by mass spectroscopy (C4−C41, C13−C33, and C20−C26), where the first two could be directly determined from NOESY cross-peaks between CHβ protons of the corresponding cysteines. The second helix contains the (L/I)^{29}IEECKTS^{36} sequence conserved in attractins from five species of *Aplysia* that could interact with the receptor. The sequence and structure of this region are similar to those of the recognition helix of the E*r*-11 pheromone of the unicellular ciliate *Euplotes raikovi*, suggesting a possible common pathway for intercellular communication of these two distinct pheromone families.

The opisthobranch mollusk *Aplysia* is a simultaneous hermaphrodite that does not normally fertilize its own eggs. The mollusks mate and lay eggs in breeding aggregations during the summer reproductive season. Following ovulation, the eggs travel to the fertilization chamber where they are mixed with mature sperm from another animal and with secretions from the albumen gland (*1*). One of the products of the albumen gland is attractin, a protein that elutes from the cordon to function as a water-borne pheromone, attracting other *Aplysia* to the area and inducing them to mate.

Approximately 1% of the cDNAs in an *Aplysia* albumen gland cDNA library encode attractin. The cDNA of *Aplysia californica* attractin encodes a signal peptide and a 58-residue protein without a transmembrane domain (*2*). The protein is degraded at the C-terminus following elution from the cordon, but this does not destroy activity, as a 47-residue fragment of the protein recovered from the seawater surrounding an egg cordon was attractive (*3*). Attractins have now been isolated from several species of *Aplysia* with overlapping and nonoverlapping geographic distributions. Where examined, attractins were cross-reactive among various *Aplysia* species, despite considerable variation in their sequences. In previous work, recombinant *A. californica* attractin expressed in insect cells was shown to be active at picomolar concentrations in T-maze attraction assays and to induce mating activity in all aquatic gastropod mollusks examined to date (*3*, *4*).

This cross-reactivity suggests that attractins, despite less than 40% overall sequence conservation, share a common three-dimensional (3D) structure and receptor-binding site. They thus provide an important biological system in which to study the mechanism of pheromone action in organisms that coordinate reproduction with signals that diffuse freely in aqueous environments. A 3D structure of the protein is essential in identifying those residues conserved in the protein family to maintain overall protein stability, and in distinguishing them from those involved in receptor binding.

The attractin sequences are not significantly similar in sequence to those of any other known protein family. Sequences are known for mating pheromones from other species, including a unicellular ciliate *Euplotes* (*5*−*7*), bacteria (*8*), yeast (*9*), algae (*10*), and amphibians (*11*).

† This work was supported by grants from the National Science Foundation (Grant DBI-9714937 to W.B. and Grant IBN-9985778 to S.D.P.), the U.S. Department of Energy (Grant DE-FG03-00ER63041 to W.B.), and the Texas Higher Education Coordinating Board Advanced Technology Program (Grant 004952-0084-1999 to W.B. and Grant 004952-0002-1999 to G.T.N.).

* To whom correspondence should be addressed: Sealy Center for Structural Biology, Department of Human Biological Chemistry and Genetics, University of Texas Medical Branch, 310 University Blvd., Galveston, TX 77555-1157. Telephone: (409) 747-6810. Fax: (409) 747-6850. E-mail: werner@newton.utmb.edu.

‡ Department of Human Biological Chemistry and Genetics.

§ The Marine Biomedical Institute and Department of Anatomy and Neurosciences.

10.1021/bi0274322 CCC: $25.00
Published on Web 07/30/2003

Despite considerable sequence diversity, NMR[1] structures of several of the pheromones from *Euplotes raikovi* (E*r*) are similar to each other, consisting of three helix bundles stabilized by three intramolecular disulfide bonds (*12*−*16*). The E*r*-23 pheromone is a five-helix bundle stabilized by five disulfide bonds (*17*). Fold recognition servers suggested that attractins could have a fold similar to that of the small E*r* pheromones. However, the level of sequence identity between the two families is low, and the pattern of disulfide bonding is different. Structures of mammalian pheromone binding proteins, including mouse urinary protein (*18*) and hamster aphrodisin (*19*), are lipocalins, primarily β-sheet proteins, and bear no resemblance to *Aplysia* attractin.

In previous work, we used molecular modeling, data from circular dichroism, and the disulfide bonds determined with mass spectroscopy to generate 3D models, using *Euplotes* pheromones E*r*-2 and E*r*-11 as templates (*4*). We present here the NMR solution structure of recombinant *Aplysia* attractin. Homonuclear two-dimensional (2D) TOCSY and a portion of the NOESY spectra were manually assigned to obtain the sequential assignment. The bulk of the NOESY peak assignments were then done simultaneously with structure calculation using self-correcting distance geometry methods implemented in our in-house suite NOAH/DIAMOD/FANTOM (*20*−*22*). In agreement with our previous models, attractin has a compact helical structure. The NMR solution structure suggests a common receptor-binding site for all attractins, which will be tested in further studies by site-directed mutagenesis. *Aplysia* attractin has a helix packing different from that of the *Euplotes* pheromones. However, the second helix of attractin, which contains a highly conserved motif, is quite similar to the third helix of the *E. raikovi* pheromone E*r*-11, which is involved in receptor recognition in the unicellular cilitate. This indicates that the exposed residues in the conserved motif in the attractins contribute to receptor binding in the mollusk.

MATERIALS AND METHODS

Recombinant Attractin Expression. The *A. californica* albumen gland attractin cDNA (*2*) was subcloned into the baculovirus expression vector pFastBac 1, and recombinant virus was generated using the Bac-to-Bac Baculovirus Expression System (Gibco BRL). Attractin was expressed in Sf9 insect cells grown in Sf-900 II serum-free medium.

Purification of Recombinant Attractin. Recombinant attractin was purified as previously described (*4*). Briefly, Sf9 cells were centrifuged, and the pellet was resuspended in ice-cold 0.1% HFBA and sonicated. The resulting lysates were purified on C18 Sep-Pak Vac cartridges (Waters) and lyophilized. The lyophilisate was purified by Vydac semi-preparative C18 RP-HPLC using a gradient of 0.1% HFBA to acetonitrile and 0.1% HFBA. The attractin-containing fractions were repurified by Vydac analytical C18 RP-HPLC using a gradient of 0.1% TFA in acetonitrile and 0.1% TFA. The peak of interest was characterized by Edman microsequence analysis and MALDI-MS, and attractin-containing fractions were pooled and lyophilized.

According to MALDI-MS, full-length recombinant attractin lacks the N-linked glycosylation at Asn8 found in the native albumen gland peptide (*3*). As both proteins are equally active in T-maze bioassays, glycosylation is not necessary for biological activity. Analysis of attractin by 20% SDS−PAGE indicated a pure protein with no high-molecular weight aggregates. The lyophilized samples were reconstituted; the pH was adjusted, and the samples were concentrated to a final attractin concentration of 0.7 mM in 10 mM sodium phosphate buffer (pH 6.8) in Centricon-3 microconcentrators (Amicon) (*4*).

NMR Experimental Details. Homonuclear ^{1}H 2D NMR experiments (TOCSY, NOESY, and DQF-COSY) at 25 and 15 °C were carried out on a Varian Unity Plus spectrometer at 600 MHz. For TOCSY and DQF-COSY, water suppression was done using the "wet-PFG" sequence. In this sequence, variable flip angle RF pulses (shaped), followed by dephasing gradient pulses, were used for water suppression. This sequence is optimized to be insensitive to T1 differences and B1 inhomogeneities across the sample (*23*, *24*). A "modified WET sequence" was used for water suppression in NOESY experiments, where the relative angles of the RF-shaped pulses were achieved by varying pulse widths rather than by varying the power levels (*25*). Good water suppression was achieved with this routine. H_2O/DSS signals were used as a reference. FELIX 2000 was used for data processing as well as for peak picking. The data were Fourier transformed using Complex FT and further processed using the Felix routine states or states−TPPI. The sinebell(60−90) window function was used for apodization.

TOCSY experiments were carried out at 15 and 25 °C using 32 scans with a mixing time of 60 ms. A spectral window of 6000 Hz was used with 2048 points in the F_2 dimension and 256 points in the F_1 dimension, and a gain of 48. NOESY experiments were also carried out at 15 and 25 °C with mixing times of 100 and 200 ms, with 2048 points in the F_2 dimension and 256 points in the F_1 dimension. DQF-COSY experiments, used to obtain *J* coupling data, were carried out with 4096 × 512 points in the F_2 and F_1 dimensions and at 15 and 25 °C. Sequential assignments were done manually using standard procedures and TOCSY, NOESY, and DQF-COSY spectra (*26*, *27*). NOE contacts between the Hβ protons of cystines were used to identify the cysteines forming disulfide bonds.

NOAH/DIAMOD Calculations. Our NOAH/DIAMOD program (*20*−*22*, *28*, *29*) was used for structure calculation and simultaneous assignment of NOESY spectra. The structure most consistent with the data is generated by automated iterative cycles of assignment and 3D structure calculation (*28*, *30*−*32*). The input data for NOAH/DIAMOD calculations were (a) protein sequence, (b) a NOESY cross-peak list with chemical shifts and their intensities, (c) angular constraints from *J* couplings or statistical data, and (d) disulfide bond constraints. The procedure that included angular constraints was previously described (*22*). Cross-peak intensities were automatically converted to upper distance constraints by the usual relation $I_{ij} = Ar^{-6}$. An upper

[1] Abbreviations: TFA, trifluoroacetic acid; HFBA, heptafluorobutyric acid; NMR, nuclear magnetic resonance; CD, circular dichroism; SDS−PAGE, sodium dodecyl sulfate−polyacrylamide gel electrophoresis; MALDI-MS, matrix-assisted laser desorption ionization mass spectrometry; DQF-COSY, double-quantum-filtered two-dimensional (2D) correlation spectroscopy; TOCSY, 2D total correlation spectroscopy; NOESY, nuclear Overhauser spectroscopy; CSI, chemical shift index; drmsd, distance root-mean-square deviation; E*r*, *E. raikovi* peptide pheromone; RP-HPLC, reverse phase high-performance liquid chromatography.

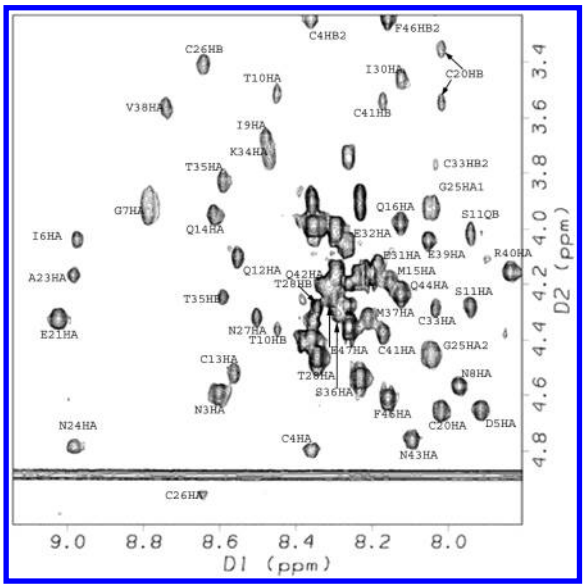

FIGURE 1: Fingerprint region of the TOCSY spectrum at 15 °C, showing most of the NH−Cα cross-peak assignments. Not all residues have chemical shifts in this region, and there are some unassigned peaks that probably arise from residues in the unstructured N- and C-terminal areas of the protein.

distance limit $r_{i,j}$ of 2.2 Å was assigned to the strongest NOESY cross-peak intensity $I_{i,j}$ to determine the constant *A*. The rest of the upper distance constraints were calculated from the inverse sixth-power law; the maximum NOE distance is taken to be 6.0 Å for non-pseudo-proton pairs. The van der Waals distances were used as lower distance limits. The manual, unambiguous, and ambiguous upper distance constraints were given relative weights of 10, 5, and 1, respectively, in the DIAMOD target function (*20*−*22*). In addition, angular constraints obtained from a statistical study of proteins for allowed ranges of backbone and χ_1 angles (*33*) were applied as previously described (*22*). A high weight factor of 10 was given to the manually assigned distance constraints in the initial NOAH/DIAMOD cycles to better assign the high number of ambiguous constraints. The chemical shift tolerance was set, at the initial cycles, restrictively to 0.010 ppm, and gradually increased to 0.025 ppm toward the later NOAH/DIAMOD cycles. In every NOAH/DIAMOD cycle, the 10 structures (of 50 total) with the lowest DIAMOD target functions were used in NOAH for the NOESY peak assignment. In the last four cycles, the 20 best structures were used. The REDAC procedure (*34*) was applied in the final cycles to increase the convergence of the bundle of structures. Floating assignments were used for diastereoscopic methylene protons that were not stereospecifically assigned.

RESULTS

Sequential Assignment

The TOCSY spectra were well-resolved, and by using two different temperatures, we were able to assign most of the spin systems, as shown in the fingerprint region of the TOCSY spectrum for the NH−CHα connectivities (Figure 1). Sequential assignments could be made for residues 3−47 on the basis of $H\alpha_{(i)}-NH_{(i+1)}$, $H\beta_{(i)}-NH_{(i+1)}$, and $H\delta_{(i)}-NH_{(i+1)}$ peaks. At least two contacts were used to confirm the sequential assignment of a residue (*26*, *27*). Cross-peaks in the amide−amide region of the NOESY spectrum were also used to confirm the sequential assignment. The number of peaks in this highly resolved area of the spectrum was consistent with the anticipated helical secondary structures in attractin (see the next section).

Although the spectra were well-resolved, some of the expected proton cross-peaks were missing or too close to

Table 1: Proton Chemical Shifts for Attractin Residues (in parts per million)

	residue	NH	αH	βH	others
1	Asp				
2	Gln				
3	Asn	8.55	4.61	2.79	γNH2, 7.66, 6.93
4	Cys	8.34	4.81	3.23, 2.92	
5	Asp	7.92	4.65	2.84, 2.73	
6	Ile	8.89	4.02	1.98	
7	Gly	8.75	3.97, 3.90		
8	Asn	7.99	4.57	2.91	γNH2, 7.84, 7.07
9	Ile	8.44	3.68	1.86	γ/δH, 1.08
10	Thr	8.44	3.52	4.36	γH, 1.18
11	Ser	7.92	4.28	4.02	
12	Gln	8.51	4.10	2.13, 2.23	γH, 2.38, 2.46
13	Cys	8.54	4.52	3.01, 3.14	
14	Gln	8.59	3.96	2.06, 2.34	γH, 2.41, 2.63; δNH2, 6.79, 7.35
15	Met	8.13	4.19	2.16, 2.26	γH, 2.65, 2.72
16	Gln	8.08	3.99	1.72, 2.27	δNH2, 7.20, 6.75
17	His	7.37	4.93	3.42, 2.8	2H, 8.10; 4H, 7.27
18	Lys	7.56	4.19	1.92, 1.98	γH, 1.41; ϵH, 3.41; ϵNH3, 7.57
19	Asn	8.25	4.93	2.91, 2.74	γNH2, 7.65, 6.92
20	Cys	8.00	4.65	3.52, 3.34	
21	Glu	8.97	4.33	2.21, 1.97	γH, 2.26, 2.33
22	Asp	7.62	4.55	2.87, 2.56	
23	Ala	8.87	4.18	1.46	
24	Asn	8.91	4.80	2.93, 2.82	γNH2, 7.60, 6.99
25	Gly	8.05	4.44, 3.94		
26	Cys	8.59	4.92	3.4, 3.05	
27	Asp	8.48	4.32	2.70	
28	Thr	8.28	4.46	4.29	γH, 1.21
29	Ile	7.54	3.87	1.77	γH, 1.05, 0.87; δH, 0.59
30	Ile	8.09	3.47	2.00	δ/γH, 0.90
31	Glu	8.16	4.12	2.15	γH, 2.44, 2.33
32	Glu	8.25	4.06	2.12	γH, 2.46, 2.22
33	Cys	8.03	4.29	3.75, 3.23	
34	Lys	8.47	3.74	1.93, 1.71	γH, 1.23; ϵH, 2.93
35	Thr	8.54	3.84	4.25	γH, 1.26
36	Ser	8.25	4.32	4.01	
37	Met	8.21	4.30	2.02, 2.33	γH, 2.89, 2.68
38	Val	8.69	3.58	2.19	γH, 1.10, 0.94
39	Glu	8.03	4.04	2.18, 2.09	γH, 2.46, 2.26
40	Arg	7.79	4.17	1.97, 1.86	γH, 1.72; δH, 3.29; NH, 7.77, 6.92
41	Cys	8.12	4.38	3.52, 3.16	
42	Gln	8.27	4.21	2.16	γH, 2.56, 2.46; δNH2, 6.82, 7.42
43	Asn	8.06	4.71	2.92, 2.84	
44	Gln	8.10	4.24	2.11	γH, 2.40
45	Glu	8.23	4.17	2.11	γH, 2.22, 1.95
46	Phe	8.11	4.62	3.22, 3.06	7.36, 7.27
47	Glu	8.28	4.26	2.04, 1.98	γH, 2.28
48	Ser				
49	Ala				
50	Ala				
51	Gly				
52	Ser				
53	Thr				
54	Thr				
55	Leu				
56	Gly				
57	Pro				
58	Gln				

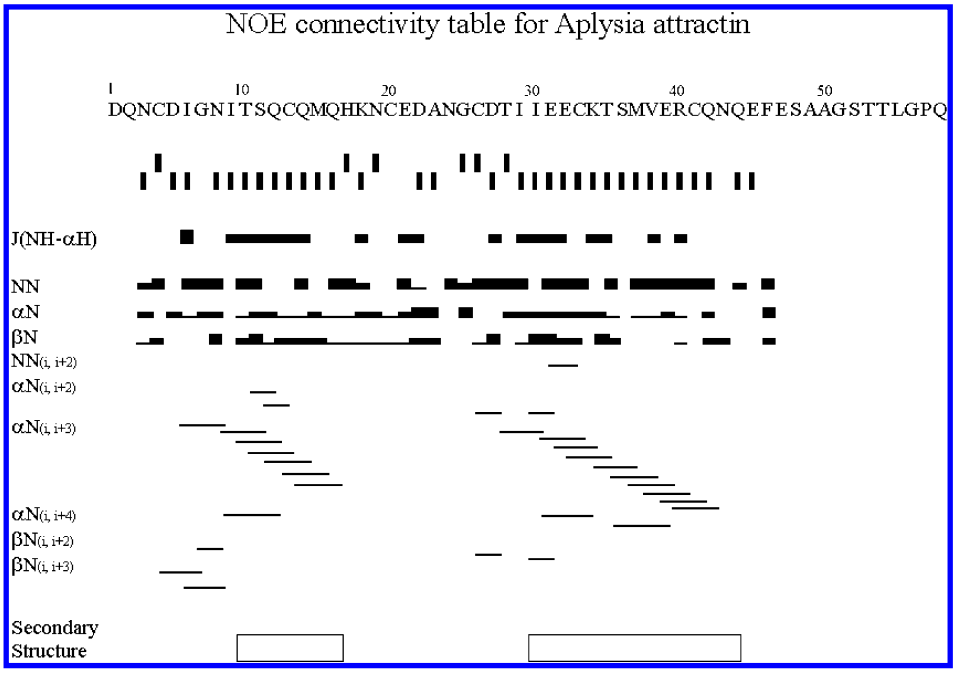

FIGURE 2: NOE connectivity table for attractin. The protein sequence is followed by the chemical shift index (CSI) for the Cα protons (on a scale of −1 to +1), the ^3J(NH−αH) values (a thick line corresponds to a J value of >10 Hz and a thin line to a J of ≤5 Hz), and the NH−NH, NH−αH, and NH−βH contacts. The next seven rows show medium-range contacts. In the lower rows of the figure, the thicknesses of the lines correlate with the intensities of the peaks. The blocks at the bottom of the picture indicate the helices found by NOAH/DIAMOD calculations.

the water line to be distinguished. For example, the cross-peaks between the amide proton of G7 and the amide and the γ or δ protons of I6 were clearly visible while the G7 NH−I6 HA cross-peak was very weak and could be seen at only very low contours. As with the TOCSY data, we were able to resolve some of the peaks where the amide chemical shifts were degenerate by comparing spectra at 15 °C. Data from a DQF-COSY spectrum were used to resolve the αH and βH protons of T10 and T28. No stereospecific assignments were made.

The chemical shifts for the different protons at 25 °C are summarized in Table 1. We were unable to detect any NOE contacts for the first two N-terminal residues and C-terminal residues 48−58. As other data indicate that the 10 C-terminal residues of the protein are highly susceptible to proteolysis (*3*, *4*), we assume that this area is more flexible than the rest of the protein.

NOE Connectivities and J Coupling Data Indicate Two Major Helical Regions in Attractin. The sequential NH−NH cross-peaks in the NOESY spectrum are indicative of an overall helical structure for attractin. Medium-range NOE contacts between $CH\alpha_{(i)}-NH_{(i+3)}$ and $CH\alpha_{(i)}-NH_{(i+4)}$, the chemical shift index (the positive or negative difference from the anticipated random coil value of the chemical shift) (*35*), and J coupling data were then used to determine which residues in the protein were most likely to be in a helical conformation. The ^3J(NH−αH) values were determined from the DQF-COSY spectrum using an automatic routine in FELIX, which uses a line-fitting algorithm to obtain the scalar couplings. These results are shown schematically in Figure 2. All the measurements are consistent with two long helical regions in attractin between residues 8−16 and 30−42. The measured ^3J(NH−αH) values (around 5 Hz in the helical regions) agree with the chemical shift data and the NOE connectivities. Few J values could be obtained in the loop region between the two helices. The last row of Figure 2 shows that the helical regions in the structures determined by NOAH/DIAMOD/FANTOM calculations (see below) are consistent with the chemical shift and J coupling data.

Confirmation of the Disulfide Bonding Pattern. Attractin has three disulfide bonds, between C4 and C41, between C13 and C33, and between C20 and C26, as determined previously by mass spectroscopic measurements after limited proteolysis (*4*). We were able to confirm the presence of the first two of these bonds, based on observed NOE peaks between Cβ protons. The cross-peak between 13Hβ and 33Hβ was observed unambiguously in the 25 °C NOESY experiment, whereas the cross-peak between 4Hβ and 41Hβ was clearest at 15 °C (Figure 3). None of the anticipated peaks for an alternative disulfide bonding pattern, such as that of the E*r* pheromones, i.e., C4−C26, C13−C41, and C20−C33, are seen in the spectrum.

Results of NOAH/DIAMOD Structure Calculations

Convergence of NOAH/DIAMOD Calculations. Initially, 136 NOESY peaks were manually assigned and kept constant during the NOAH/DIAMOD calculations. These were for the most part those NOE peaks indicating contact between adjacent residues used for the sequential assignment, and a small number of medium-range and intraresidue contacts. The rest of the NOE peaks were assigned automatically in NOAH/DIAMOD. The number of NOESY cross-peaks that were assigned increased rapidly during the first 30 NOAH/DIAMOD cycles and then leveled off (Figure 4). At the end of 74 cycles, NOAH assigned 813 peaks unambiguously and 110 peaks with more than one possible assignment, consistent with the final structure and the chemical shift tolerance. A total of 949 peaks, including the initial manual assignments, were unambiguously assigned which corresponds to 79% of all NOESY cross-peaks in the peak list. The convergence

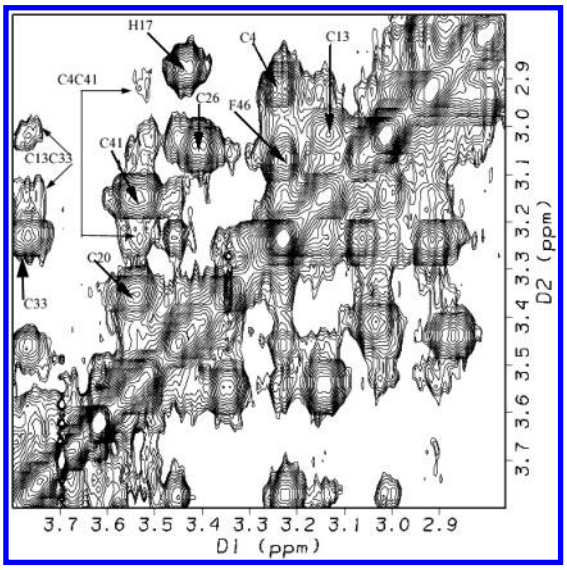

FIGURE 3: Disulfide bond cross-peaks seen in NOESY spectra. A portion of the NOESY spectrum (200 ms, 25 °C) is shown, illustrating the short 13Hβ−33Hβ contact consistent with a disulfide bridge between these cysteines. The C13−C33 and C4−C41 interresidue connectivities are labeled with double-headed arrows, whereas the intraresidue cross-peaks of the cysteines are labeled with single-headed arrows.

of the bundle of structures during the NOAH/DIAMOD cycles is also demonstrated in Figure 4 as the average spread in the pairwise drmsd between the structures. The drmsd, calculated for residues 11−42, falls to 0.74 Å after 50 cycles.

The final structures after the NOAH/DIAMOD calculations are most constrained between residues 3 and 47. The structures were seen to have, in general, two α-helical regions, between T10 and Q16 and between I30 and E38. The helical regions were essentially identical in all calculations with good fits between different sets of calculations. An additional minor conformation of the loop region was observed depending on NOAH/DIAMOD parameters. Figure 5 shows the ensemble of 20 structures with the smallest target function, averaged to the mean structure after 74 NOAH/DIAMOD cycles. For residues 3−47, the rmsd was 0.58 ± 0.05 Å for backbone atoms and 1.17 ± 0.07 Å for heavy atoms. For helical region I, these values for backbone and heavy atoms were 0.16 ± 0.04 and 0.67 ± 0.09 Å, respectively. For helix II, the corresponding values were 0.12 ± 0.04 and 0.73 ± 0.14 Å, respectively. The values for the loop region were 0.56 ± 0.08 and 1.06 ± 0.12 Å, respectively.

FANTOM Energy Minimization of NOAH/DIAMOD Structures. The bundle of 20 structures with the smallest target functions from NOAH/DIAMOD were refined using energy minimization with our FANTOM program. Table 2 shows the values of the energy terms (conformational, electric, H-bond, Lennard-Jones, etc.) before and after FANTOM minimization. All energy terms decreased during the minimization, and the average rmsd among the energy-refined structures, 0.72 ± 0.12 Å for backbone atoms and 1.32 ± 0.11 Å for heavy atoms for residues 3−47, was slightly higher than that for the starting structures. Only distance constraints from unambiguously assigned NOESY cross-peaks were used in the restrained energy minimization, whereas in the NOAH/DIAMOD calculations, ambiguously assigned NOESY cross-peaks also contribute.

Validation of the Structure. The Ramachandran plot for all 20 models and for residues 3−47 was plotted using AQUA/Procheck_NMR (*36*, *37*). The ϕ and ψ dihedral angles of 98% of all residues from all the models occupy the generously allowed region, showing that the 3D structures are overall stereochemically acceptable.

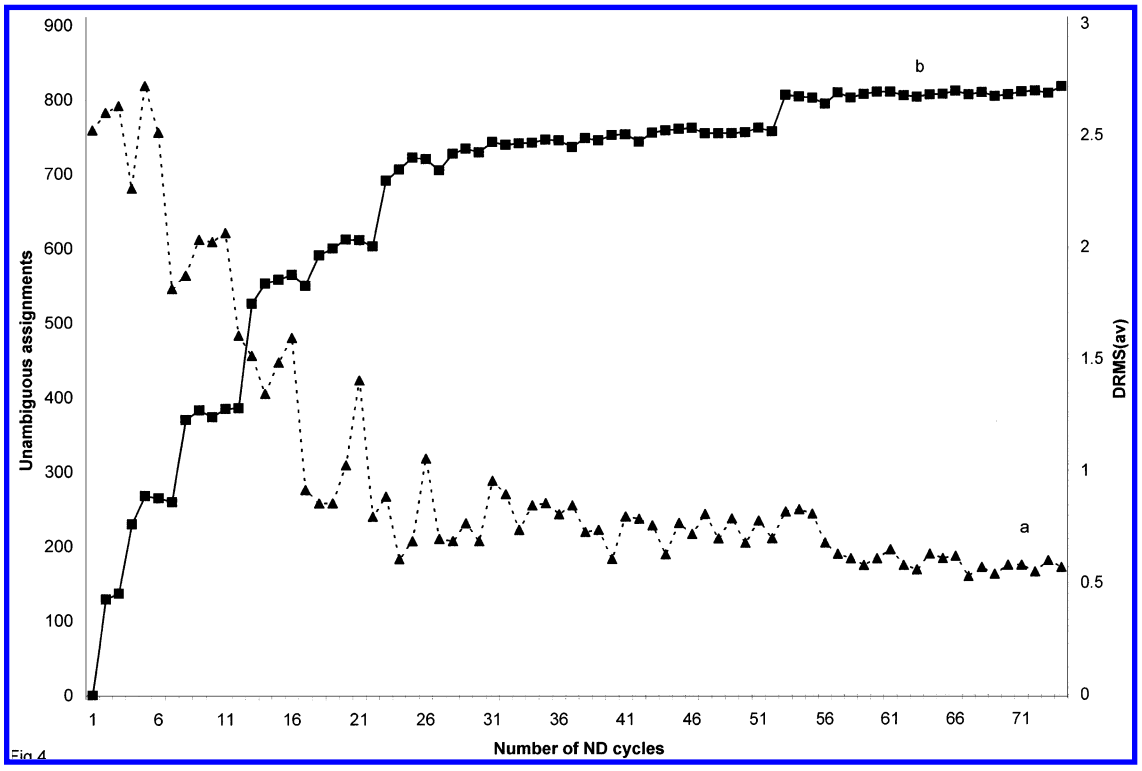

FIGURE 4: Convergence of the automatic structure calculation. (a) Peak assignments (UAL) (■) and (b) average spreads in the pairwise drmsd between the structures (▲) are plotted as a function of the number of NOAH/DIAMOD cycles.

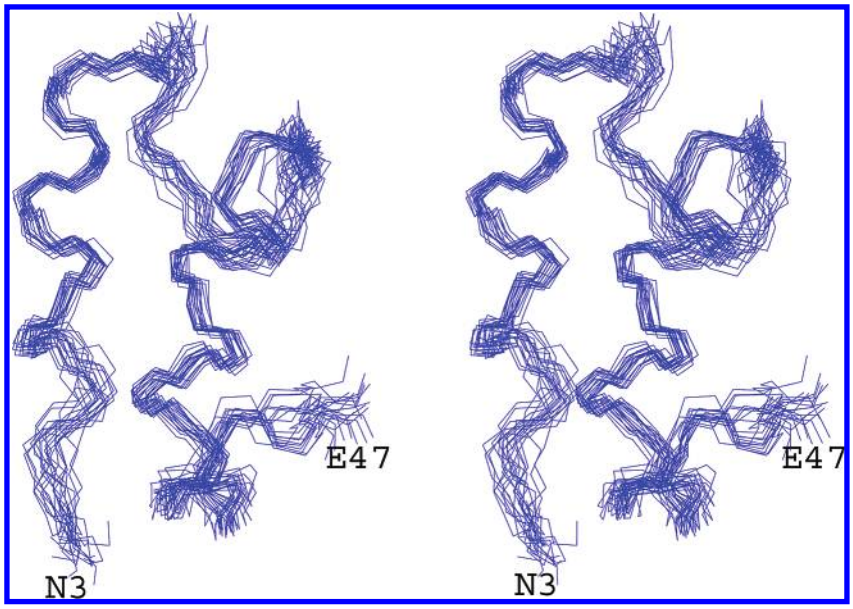

FIGURE 5: Bundle of 20 structures with the smallest target function from a NOAH/DIAMOD calculation (only the backbones are shown for residues 8−42).

Table 2: Summary of Structure Calculation Results

no. of NOESY peaks used	1200
no. of fixed assignments (manual)	136
no. of peaks assigned by NOAH unambiguously	813
no. of peaks assigned by NOAH ambiguously	110
no. of unambiguous constraints after ND calculations	946
no. of constraints used by FANTOM	880

	energy (kcal/mol)[a]			
	conformational	electric	H-bond	Lennard-Jones
initial	711 ± 74	29 ± 12	−9 ± 39	463 ± 66
final	−301 ± 35	−21 ± 9	−86 ± 7	−284 ± 23

residues	rmsd after FANTOM energy minimization (Å)
3−47 and backbone	0.72 ± 0.12
3−47 and heavy atoms	1.32 ± 0.11
10−16 and 30−38 and backbone	0.35 ± 0.06
10−16 and 30−38 and heavy atoms	0.84 ± 0.10
18−29 and backbone	0.57 ± 0.08
18−29 and heavy atoms	1.08 ± 0.14

[a] Thirteen constraint violations of >1.00 Å in at least 10 structures. Five angle constraint violations of >10.00° in at least 15 structures.

We also examined the influence of the total number of calculated structures and the number of selected structures in the NOAH cycles on the resulting final structures. Two additional calculations, set 2 and set 3, were carried out, and compared to the original parameter settings as described in Materials and Methods (set 1). In set 2, we increased the total number of structures calculated at each NOAH/DIAMOD cycle from 50 to 99, and kept all other parameters as in set 1. In set 3, we used the same total number of structures as in set 2, and gradually increased the number of structures selected for the NOAH assignments from 10 up to 40 at the final cycle. The convergence toward the final bundle of structures only changed slightly with rmsd values of backbone residues 3−47 within the bundles of the final set 2 structures of 0.68 and 0.79 Å for set 3 structures, as compared to 0.57 Å for the original calculation with set 1. The three mean structures of the three sets have the same helix topology as described for set 1 with a mean value of the pairwise rmsd of 0.61 Å for the well-defined region comprising the segments of residues 10−16 and 30−38, and 1.27 Å for residues 3−47.

Hydrophobic Core and Solvent-Exposed Residues of the Aplysia Attractin Solution Structure. Residues forming the core of attractin, that is, those with less than 20% surface exposure of side chains in the mean structure, were determined with our GETAREA program (*38*) (Figure 6). These include the cysteines forming the two disulfide bonds (C4−C41 and C13−C33) and residues I9, T10, Q14, I30, and V38. Most of these residues are hydrophobic or have a large nonpolar side chain. We have excluded residues from this list if their side chains are mainly unstructured, such as all residues from position 43 to 58, and K18 and A23 in the loop region. K34 has a small exposed surface area in the mean structure as it is covered from residues of the unstructured C-terminal end. Several residues conserved in the known attractin sequences (*4*), indicated with asterisks in Figure 6, and which are more than 50% surface-exposed, such as D5, S11, M15, E31, E32, and E39, may contribute to receptor binding. Their role in biological activity will be tested by site-directed mutagenesis.

Figure 7 shows the NMR solution structure of attractin, represented by the conformer with the smallest rmsd from the mean structure. The two helical regions (T10−M16 and I30−V38) are packed in an antiparallel conformation separated by a loop region. The C13−C33 disulfide bond and residues I9, T10, I30, and V38 make contacts between the two helices, to form the hydrophobic core. These residues also have many NOE contacts to neighboring residues. The potential receptor binding site (L/I)^{29}IEECKTS^{36} and several other residues conserved in five different attractins (*4*) are surface-exposed (Figure 7).

A Conserved Area Similar in Sequence and Structure to the Recognition Helix of the Er Pheromones. Overall, the attractin structure represents a new fold. The DALI Webserver (*39*) found no other comparable protein fold in the Protein Data Bank with a *Z* score of ≥2. However, there is

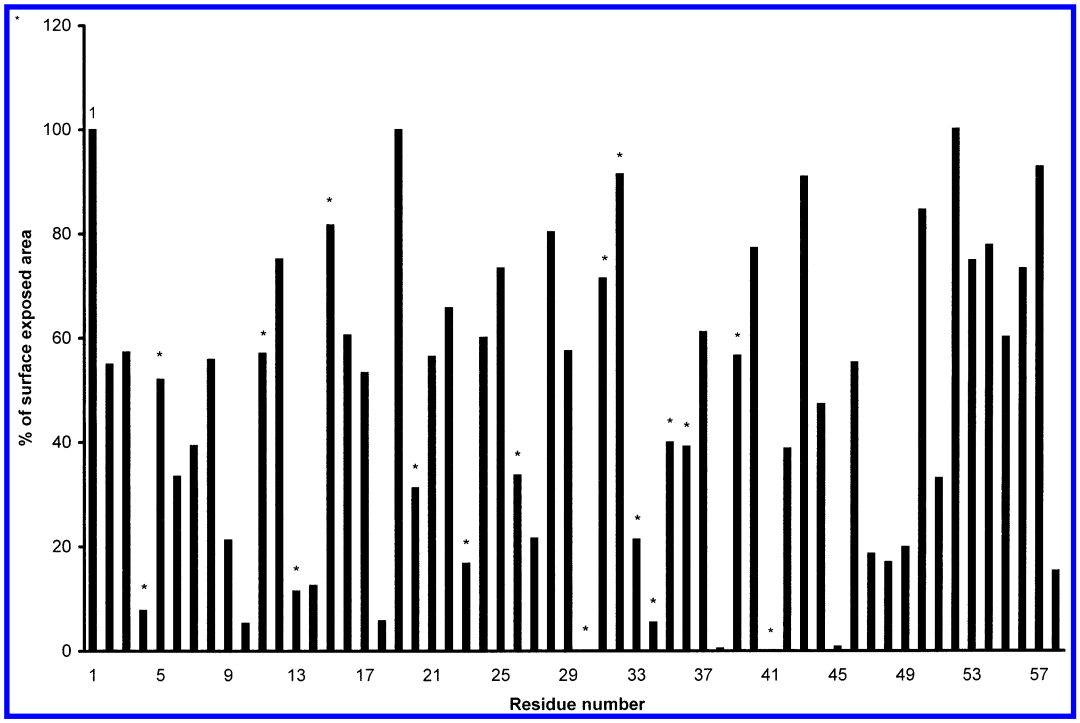

FIGURE 6: Solvent-exposed and buried residues of the NMR solution structure of attractin. The fraction of solvent-exposed side chain area relative to this area in random coil conformations was calculated for the mean structure using the GETAREA program (*38*). Residues labeled with asterisks are conserved among all five known attractins (*4*).

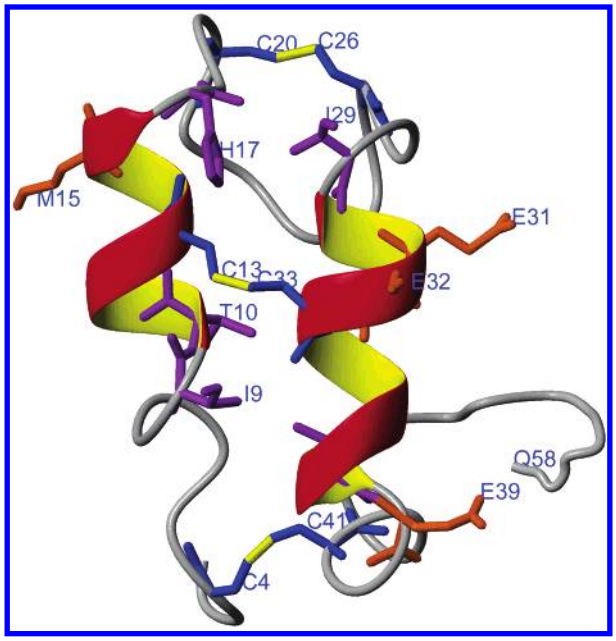

FIGURE 7: Ribbon representation of one of the representative structures (those with the smallest rmsds from the mean) with the side chains of core residues (magenta) and conserved solvent-exposed residues (orange). The disulfide bonds between cysteines (yellow) and the helical regions of residues T10−Q16 and I30−V38 are also shown in this structure.

some local resemblance of the attractin structure to the small *Euplotes* pheromones that we previously used as modeling templates (*4*), especially in the area that is considered the recognition helix of the E*r* pheromones (*40*, *41*). The "bestfit" program of Swiss PDB viewer determined an rmsd of 1.3 Å over 48 backbone atoms for residues T28−M37, R40, and C41 of attractin to residues P21−V30, E35, and E36 of E*r*-11 (PDB entry 1ERY) without specifying the corresponding

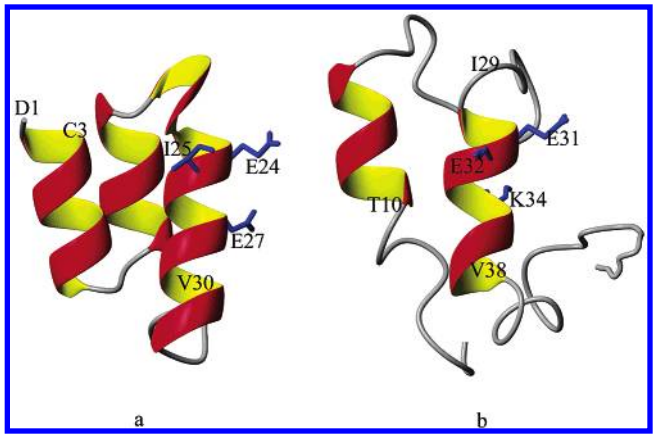

FIGURE 8: Comparison of the mean NMR structures of the E*r*-11 pheromone (a) and *Aplysia* attractin (b). The third helix of E*r*-11 (I23−V30) and the second helix of attractin (I30−V38) are similar in the backbone and the orientation of conserved side chains.

regions. The structural similarity between the potential binding surfaces of the *Aplysia* attractin and E*r*-11 is illustrated in Figure 8. The bestfit program did not find any matching area between attractin and 10 other helical protein structures, including those for many four-helix bundle cytokines and the chemokine interleukin 8.

DISCUSSION

The NMR solution structure of *A. californica* attractin provides the opportunity to better understand pheromone communication among marine animals and to analyze, at the molecular level, signaling that regulates their reproductive behavior. The current study verifies the hypothesis of our previous modeling studies that the protein is mainly α-helical (*4*). The helix packing of the experimental NMR structure is, however, different from that of our models. The two

helices in the solution structure are very well defined, with bundle rmsd values from the mean of less than 0.5 Å. In contrast, the last 11 amino acids are unstructured as previously suggested by their sensitivity to the proteolytic digest of attractin *in vivo* and *in vitro* (*3*, *4*).

The robustness of our NMR bundle of structures was tested by varying the number of total and selected structures in the NOAH/DIAMOD approach in calculations set 1, set 2, and set 3. The convergence of the structures in these three calculations was comparable in quality, and the mean structures of the bundles changed only slightly in the well-defined regions. In previous studies on the NMR structure of the New World Scorpion neurotoxin (*22*) and of the myeloid progenitor inhibitory factor-1 (*42*), we also assessed the influence of distance calibration on the quality of structures. In that study, we compared the 3D structures obtained by our NOAH/DIAMOD method to those structures obtained by standard manual assignment and restrained MD calculations with a simple three-level calibration with generous upper bounds for strong, medium, and weak cross-peaks. In both calculations, we showed that the 3D structures obtained by our distance calibration and of the manual method using more generous upper bounds do not significantly deviate, proving that the effect of distance calibration is not substantial.

Common Surface-Exposed Residues: A Basis for Cross-Reactivity of Aplysia Pheromones? Attractin-related peptides have been characterized from five species of *Aplysia* (*43*, *44*), including *Aplysia brasiliana* (PIR entry B59060), *Aplysia fasciata* (PIR entry A59447), *Aplysia depilans* (PIR entry A59446), and *Aplysia vaccaria* (PIR entry A59424), which are 94, 91, 35, and 33% identical in sequence, respectively, to *A. californica* attractin (PIR entry A59061). All five of these attractins have in common six cysteines and a motif, corresponding to $(L/I)^{29}$IEECKTS^{36} in the *A. californica* attractin, features that probably account for their ability to cross-react in T-maze assays. More recent data indicate that attractins from other mollusks may have a similar receptor site. The attractin of *Bursatella* (PIR entry 59453), an opisthobranch mollusk that belongs to a subfamily different from that of *Aplysia*, is only 20% identical to *A. californica* attractin but shares the same pattern of six cysteine residues and three residues that correspond to D5, E31, and E32 (manuscript in preparation).

The attractin solution structure allows us to separate residues conserved for structural reasons across *Aplysia* species, such as the cysteines or the core residue I30, from those such as D5, S11, M15, E31, E32, and E39, whose surface exposure could reflect a role in receptor recognition. Site-directed mutagenesis of these residues will be done to test their effect on biological activity. The structure can also serve as a basis for modeling the structure of more distantly related attractins, such as that from *Bursatella*. Future *in vivo* studies with *Bursatella* attractin will aid in determining the importance of particular residues for attraction and/or mating activity.

Similarity to the Recognition Helix of Euplotes Pheromones. Attractin, according to DALI, has an overall fold different from those of others in the Protein Data Bank. As noted above (Figure 8), the conserved motif of the attractins matches structurally the third helix region of the E*r*-11 pheromone. This attractin helix also has a low backbone rmsd with respect to the third helix in the other related *Euplotes* pheromone structures (data not shown), which have less identical sequences. We consider this structural similarity significant, as it matches the area that on the basis of sequence conservation is most likely to be involved in attractin function, with the receptor recognition helix of the E*r* family (*40*, *41*). The E*r* pheromones stimulate both cell proliferation and mating pair formation in the ciliates that produce them (*45*). While they differ greatly in their mature primary sequence, with only the six cysteines and an N-terminal aspartic acid that is absolutely conserved, all have the same compact "pyramid" 3D structure of three α-helices stabilized by three disulfide bonds (*14*, *15*, *40*, *41*, *46*). Future studies on the mechanism of attractin action in mollusks and higher species should indicate whether attractin represents an evolutionary link between the protein-based pheromones of unicellular organisms and the intercellular signaling proteins of higher organisms.

Pheromones in Mammals. The most studied odorants and/or pheromones in mammals are small volatile molecules, such as aliphatic carboxylic acids or alcohols, farnasenes, and N- and S-containing unsaturated ring compounds (*47*, *48*). Mammalian lipocalins, including mouse major urinary protein (*18*) and aphrodisin (*19*), were originally described as pheromone binding proteins, and a hydrophobic binding pocket for known pheromones was distinguished in the structures. More recently, data have accumulated that indicate that recombinant pheromone binding proteins have pheromonal activity on their own, and that the pheromones may be detected indirectly, by changes they induce in the binding protein (*48*). The crystal structure of aphrodisin revealed a "serendipitous ligand" of unknown chemical nature, apparently scavenged from the bacterial host, in the pheromone binding pocket, which the authors suggest could aid in the protein's ability to cause a response in male hamster (*19*). Attractin is smaller, and its 3D structure is different from that of lipocalins, which are primarily β-sheets. Also, there is no clear intramolecular hydrophobic pocket for binding small molecules. Mass spectroscopic measurements of attractin (*4*) indicate there are no additional molecules bound to purified recombinant attractin. However, this result does not eliminate the possibility that attractin binds to small molecules, produced by the mollusks or present in artificial seawater, to exert its activity in the biological assay.

Attractin: A Possible Link between Unicellular and Multicellular Signaling Proteins. The similarity of attractins to the E*r* pheromones raises yet another interesting feature of the attractin system. The E*r*-1 pheromone can bind to the mammalian cell receptor for IL-2 (*49*), raising the intriguing possibility that pheromones may be the ancestors of the signaling proteins, cytokines, in higher organisms. Many proteins that serve as intercellular messengers in mammals, including growth hormones and cytokines such as IL-2, IFNs, and the colony stimulating factors, are helical bundles (*50*). There is immunological evidence of the existence of cytokine-like molecules and their receptors in *Aplysia* (*51*), and feline IFN-ω protects pearl oysters from virus (*52*, *53*). There is, however, no obvious sequence similarity between attractins and cytokines. Further studies of attractin's mechanism of stimulation in the mollusk will be needed to clarify possible similarities in signaling pathways.

CONCLUSIONS

We describe the first experimentally determined structure of a pheromone protein from a marine organism, *Aplysia* attractin. The NMR solution structure of attractin indicates two large helices, with disulfide bonds between cysteines C4 and C41, C13 and C33, and C20 and C26, consistent with previous biophysical evidence. On the basis of sequence analysis and the NMR solution structure, we suggest a specific group of residues, common to the known *Aplysia* attractins, to account for biological activity. Similarities between the attractin structure and those of small ciliate pheromones suggest a possible common, ancient pathway for intercellular communication mediated by protein pheromones.

ACKNOWLEDGMENT

We thank Bret Clough for expert technical assistance, and acknowledge the University of Texas Medical Branch (UTMB) Protein Chemistry Cancer Center, which is supported by the UTMB Educational Cancer Center, for Edman microsequence analyses.

REFERENCES

1. Coggeshall, R. E. (1972) The structure of the accessory genital mass in *Aplysia californica*, *Tissue Cell 4*, 105−127.
2. Fan, X., Wu, B., Nagle, G. T., and Painter, S. D. (1997) Molecular cloning of a cDNA encoding a potential water-borne pheromonal attractant released during *Aplysia* egg laying, *Mol. Brain Res. 48*, 167−170.
3. Painter, S. D., Clough, B., Garden, R. W., Sweedler, J. V., and Nagle, G. T. (1998) Characterization of *Aplysia* attractin, the first water-borne peptide pheromone in invertebrates, *Biol. Bull. 194*, 120−131.
4. Schein, C. H., Nagle, G. T., Page, J. S., Sweedler, J. V., Xu, Y., Painter, S. D., and Braun, W. (2001) *Aplysia* attractin: biophysical characterization and modeling of a water-borne pheromone, *Biophys. J. 81*, 463−472.
5. Raffioni, S., Luporini, P., Chait, B. T., Disper, S. S., and Bradshaw, R. A. (1988) Primary structure of the mating pheromone E*r*-1 of the ciliate *Euplotes raikovi*, *J. Biol. Chem. 263*, 18152−18159.
6. Raffioni, S., Luporini, P., and Bradshaw, R. A. (1989) Purification, characterization, and amino acid sequence of the mating pheromone, E*r*-10 of the ciliate *Euplotes raikovi*, *Biochemistry 28*, 5250−5256.
7. Raffioni, S., Miceli, C., Vallesi, A., Chowdhury, S. K., Chait, B. T., Luporini, P., and Bradshaw, R. A. (1992) The primary structure of *E. raikovi* pheromones: a comparison of five sequences of pheromones from cells with variable mating interactions, *Proc. Natl. Acad. Sci. U.S.A. 89*, 2071−2075.
8. Wu, K. P., An, F. Y., and Clewell, D. B. (1999) *Enterococcus faecalis* pheromone-responding plasmid pAD1 gives rise to an aggregation (clumping) response when cells are exposed to subinhibitory concentrations of chloramphenicol, erythromycin, or tetracycline, *Plasmid 41*, 82−88.
9. Kamiya, Y., Sakurai, A., Tamura, S., Takahashi, N., Abe, K., Tsuchiya, E., Fukui, S., Kitada, C., and Fujino, M. (1978) Structure of rhodotorucine A, a novel lipopeptide, inducing mating tube formation in *Rhodosporidium toruloides*, *Biochem. Biophys. Res. Commun. 83*, 1077−1083.
10. Sekimoto, H., Fukumoto, R., Dohmae, N., Takio, K., Fujii, T., and Kamiya, Y. (1998) Molecular cloning of a novel sex pheromone responsible for the release of a different sex pheromone in *Closterium peracerosum-strigosum-littorale* complex, *Plant Cell Physiol. 39*, 1169−1175.
11. Kikuyama, S., Toyoda, F., Ohmiya, Y., Matsuda, K., Tanaka, S., and Hayashi, H. (1995) Sodefrin: a female-attracting peptide pheromone in newt cloacal glands, *Science 267*, 1643−1645.
12. Brown, L. R., Mronga, S., Bradshaw, R. A., Ortenzi, C., Luporini, P., and Wüthrich, K. (1993) Nuclear magnetic resonance solution structure of the pheromone E*r*-10 from the ciliated protozoan *Euplotes raikovi*, *J. Mol. Biol. 231*, 800−816.
13. Ottiger, M., Szyperski, T., Luginbühl, P., Ortenzi, C., Luporini, P., Bradshaw, R. A., and Wüthrich, K. (1994) The NMR solution structure of the pheromone E*r*-2 from the ciliated protozoan *Euplotes raikovi*, *Protein Sci. 3*, 1515−1526.
14. Mronga, S., Luginbühl, P., Brown, L. R., Ortenzi, C., Luporini, P., Bradshaw, R. A., and Wüthrich, K. (1994) The NMR solution structure of the pheromone E*r*-1 from the ciliated protozoan *Euplotes raikovi*, *Protein Sci. 3*, 1527−1536.
15. Luginbühl, P., Wu, J., Zerbe, O., Ortenzi, C., Luporini, P., and Wüthrich, K. (1996) The NMR solution structure of the pheromone E*r*-11 from the ciliated protozoan *Euplotes raikovi*, *Protein Sci. 5*, 1512−1522.
16. Liu, A. Z., Luginbühl, P., Zerbe, O., Ortenzi, C., Luporini, P., and Wüthrich, K. (2001) NMR structure of pheremone E*r*-22 from *Euplotis raikovi*, *J. Biomol. NMR 19*, 75−78.
17. Zahn, R., Damberger, F., Ortenzi, C., Luporini, P., and Wüthrich, K. (2001) NMR structure of the *Euplotes raikovi* pheromones E*r*-23 and identification of its five disulphide bonds, *J. Mol. Biol. 313*, 923−931.
18. Luecke, C., Franzoni, L., Abbate, F., Loehr, F., Ferrari, E., Sorbi, R. T., Rueterjans, H., and Spisni, A. (1999) Solution structure of a recombinant mouse major urinary protein, *Eur. J. Biochem. 266*, 1210−1218.
19. Vincent, F., Loebel, D., Brown, K., Spinelli, S., Grote, P., Breer, H., Cambilau, C., and Tegoni, M. (2001) Crystal structure of aphrodisin, a sex pheromone from female hamster, *J. Mol. Biol. 305*, 459−469.
20. Xu, Y., Wu, J., Gorenstein, D., and Braun, W. (1999) Automated 2D NOESY assignment and structure calculation of crambin (S22/I25) with the self-correcting distance geometry based NOAH/DIAMOD programs, *J. Magn. Reson. 136*, 76−85.
21. Xu, Y., Schein, C. H., and Braun, W. (1999) Combined automated assignment of NMR spectra and calculation of three-dimensional protein structures, in *Biological Magnetic Resonance* (Berliner, L. J., and Rama Krishna, N., Eds.) pp 37−79, Plenum Publishers, New York.
22. Xu, Y., Jablonsky, M. J., Jackson, P. L., Braun, W., and Krishna, N. R. (2001) Automatic assignment of NOESY cross peaks and determination of the protein structure of a new world scorpion neurotoxin using NOAH/DIAMOD, *J. Magn. Reson. 148*, 35−46.
23. Ogg, R. J., Kingsley, P. B., and Tylor, J. S. (1994) WET, a T1- and B1-insensitive water-suppression method for in vivo localized ^{1}H NMR spectroscopy, *J. Magn. Reson. 104*, 1−10.
24. Smallcombe, S. H., Patt, S. L., and Keifer, P. A. (1995) WET solvent suppression and its applications to LC NMR and high-resolution NMR spectroscopy, *J. Magn. Reson. 117*, 295−303.
25. Zhang, S. M., Yang, X., and Gorenstein, D. G. (2000) Enhanced suppression of residual water in a "270" WET sequence, *J. Magn. Reson. 143*, 382−386.
26. Wüthrich, K. (1986) *NMR of Proteins and Nucleic Acids*, Wiley-Interscience, New York.
27. Redfield, C. (1996) Resonance assignment for small molecules, in *NMR of Macro Molecules: A Practical Approach* (Roberts, G. C. K., Ed.) Oxford University Press, Leicester, U.K.
28. Mumenthaler, C., and Braun, W. (1995) Automated assignment of simulated and experimental NOESY spectra of proteins by feedback filtering and self-correcting distance geometry, *J. Mol. Biol. 254*, 465−480.
29. Mumenthaler, C., Güntert, P., Braun, W., and Wüthrich, K. (1997) Automated combined assignment of NOESY spectra and three-dimensional protein structure determination, *J. Biomol. NMR 10*, 351−362.
30. Braun, W., and Go, N. (1985) Calculation of protein conformations by proton−proton distance constraints: a new efficient algorithm, *J. Mol. Biol. 186*, 611−626.
31. Braun, W. (1987) Distance geometry and related methods for protein-structure determination from NMR data, *Q. Rev. Biophys. 19*, 115−157.
32. Hänggi, G., and Braun, W. (1994) Pattern recognition and self-correcting distance geometry calculations applied to myohemerythrin, *FEBS Lett. 344*, 147−153.
33. Abagyan, R., and Totrov, M. (1994) Biased probability Monte Carlo conformational searches and electrostatic calculations for peptides and proteins, *J. Mol. Biol. 235*, 983−1002.
34. Güntert, P., and Wüthrich, K. (1991) Improved efficiency of protein structure calculations from NMR data using the program DIANA with redundant dihedral constraints, *J. Biomol. NMR 1*, 447−456.

35. Wishart, D. S., Sykes, B. D., and Richards, F. M. (1992) The chemical shift index: a fast and simple method for the assignment of proton secondary structure through NMR spectroscopy, *Biochemistry 31*, 1647−1651.
36. Laskowski, R. A., MacArthur, M. W., Moss, D. S., and Thornton, J. M. (1993) PROCHECK: a program to check the stereochemical quality of protein structures, *J. Appl. Crystallogr. 26*, 283−291.
37. Laskowski, R. A., Rullmann, J. A. C., MacArthur, M. W., Kaptein, R., and Thornton, J. M. (1996) AQUA and PROCHECK-NMR: programs for checking the quality of protein structures solved by NMR, *J. Biomol. NMR 8*, 477−486.
38. Fraczkiewicz, R., and Braun, W. (1998) Exact and efficient analytical calculation of the accessible surface areas and their gradients for macromolecules, *J. Comput. Chem. 19*, 319−333.
39. Holm, L., and Sander, C. (1996) Alignment of three-dimensional protein structures: network server for database searching, *Methods Enzymol. 266*, 653−662.
40. Weiss, M. S., Anderson, D. H., Raffioni, S., Bradshaw, R. A., Ortenzi, C., Luporini, P., and Eisenberg, D. (1995) A cooperative model for receptor recognition and cell-adhesion: evidence from the molecular packing in the 1.6-Å crystal structure of the pheromone E*r*-1 from the ciliated protozoan *Euplotes raikovi*, *Proc. Natl. Acad. Sci. U.S.A. 92*, 10172−10176.
41. Luporini, P., Miceli, C., Ortenzi, C., and Vallesi, A. (1996) Ciliate pheromones, *Prog. Mol. Subcell. Biol. 17*, 80−104.
42. Oezguen, N., Adamian, L., Xu, Y., Rajarathnam, K., and Braun, W. (2002) Automated assignment and 3D structure calculations using combinations of homonuclear and 3D heteronuclear NOESY spectra, *J. Biomol. NMR 22*, 249−263.
43. Painter, S. D., Akalal, D.-B. G., Clough, B., Susswein, A. J., Levy, M., and Nagle, G. T. (2000) Characterization of four new members of the attractin family of peptide pheromones in *Aplysia*, *Soc. Neurosci. Abstr. 26*, 1166.
44. Painter, S. D., Clough, B., Black, S., and Nagle, G. T. (2003) Behavioral characterization of attractin, a water-borne peptide pheromone in the genus *Aplysia*, *Biol. Bull.* (in press).
45. Ortenzi, C., Alimenti, C., Vallesi, A., Di Pretoro, B., La Terza, A., and Luporini, P. (2000) The autocrine mitogenic loop of the ciliate *Euplotes raikovi*: the pheromone membrane-bound forms are the cell binding sites and potential signaling receptors of soluble pheromones, *Mol. Biol. Cell 11*, 1445−1455.
46. Miceli, C., La Terza, A., Bradshaw, R. A., and Luporini, P. (1991) Structural characterization of mating pheromone precursors of the ciliate protozoan *Euplotes raikovi*. High conservation of pre and pro regions versus high variability of secreted regions, *Eur. J. Biochem. 202*, 759−764.
47. Buck, L. B. (2000) The molecular architecture of odor and pheromone sensing in mammals, *Cell 100*, 611−618.
48. Novotny, M. V. (2003) Pheromones, binding proteins and receptor responses in rodents, *Biochem. Soc. Trans. 31*, 117−122.
49. Vallesi, A., Giuli, G., Ghiara, P., Scapigliati, G., and Luporini, P. (1998) Structure−function relationships of pheromones of the ciliate *Euplotes raikovi* with mammalian growth factors: cross-reactivity between E*r*-1 and interleukin-2 systems, *Exp. Cell Res. 241*, 253−259.
50. Schein, C. H. (2002) The shape of the messenger: using protein structure information to design novel cytokine-based therapeutics, *Curr. Pharm. Des. 8*, 2113−2129.
51. Hughes, T. K., Jr., Smith, E. M., Leung, M. K., and Stefano, G. B. (1992) Evidence for the conservation of an immunoreactive monokine network in invertebrates, *Ann. N.Y. Acad. Sci. 650*, 74−80.
52. Kitamura, S., Jung, S., and Suzuki, S. (2000) Seasonal change of infective state of marine birnavirus in Japanese pearl oyster *Pinctada fucata*, *Arch. Virol. 145*, 2003−2014.
53. Kitamura, S., Tomaru, Y., Kawabata, Z., and Suzuki, S. (2002) Detection of marine birnavirus in the Japanese pearl oyster *Pinctada fucata* and seawater from different depths, *Dis. Aquat. Org. 50*, 211−217.

BI0274322